THE JOURNAL OF PHYSICAL CHEMISTRY B

Article

pubs.acs.org/JPCB

Simulations of Polyelectrolyte Adsorption to a Dielectric Like-Charged Surface

Alexandre P. dos Santos,* Matheus Girotto,* and Yan Levin*

Instituto de Física, Universidade Federal do Rio Grande do Sul, Caixa Postal 15051, CEP 91501-970 Porto Alegre, RS, Brazil

ABSTRACT: We explore, using the recently developed efficient Monte Carlo simulation method, the interaction of an anionic polyelectrolyte solution with a like-charged dielectric surface. In addition to polyions, the solution also contains salt with either monovalent, divalent, or trivalent counterions. In agreement with recent experimental observations, we find that multivalent counterions can lead to strong adsorption of polyions onto the surface. On the other hand, addition of a 1:1 electrolyte diminishes the adsorption induced by the multivalent counterions. Dielectric discontinuity at the interface is found to play only a marginal role in polyion adsorption.

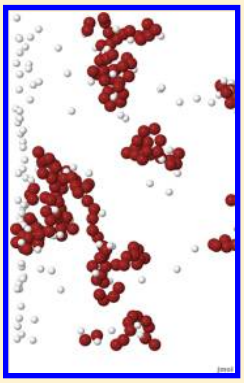

INTRODUCTION

Charged polymers are ubiquitous in biology and chemistry. In industry, they are used as purifying agents[1,2] and super-absorbents. The strong electrostatic attraction between charged impurities, induced by the oppositely charged polyions, can lead to flocculation and precipitation of suspensions. Polyelectrolytes are also used in medical applications as antibiotics[3−7] and in diagnostics as chemical sensors.[8,9] For amphiphilic polyelectrolytes the antimicrobial behavior appears to be related to the electrostatic interactions between the negative charges of the cell membrane and positive charges of the polyion, as well as the hydrophobic interactions between the phospholipids and polyelectrolytes. Under physiological conditions, DNA is a negatively charged polyion that can interact with positively charged liposomes or proteins. A number of groups have studied charged polymers interacting with oppositely charged surfaces,[10−18] with special attention given to the curvature effects.[19,20] Ionic specificity, the so-called Hofmeister effect, was observed in the interaction between polyions and hydrophobic surfaces.[21−23] Other authors have investigated the effective attraction induced by multivalent counterions between like-charged polyions.[24−30] This attraction was found to be short-ranged and to depend strongly on the concentration of multivalent counterions and monovalent salts present in the solutions. The attraction appeared as a consequence of strong positional correlations between the condensed counterions surrounding the polyions.[31] Recently, some groups conducted studies on the interaction between polyelectrolytes and like-charged membranes,[32−34] which is also the topic of the present paper. In the present work, we will explore the effect of dielectric contrast and the concentration of both multivalent and monovalent electrolytes on the interaction of polyelectrolytes with a like-charged surface.

Simulations of Coulomb systems are difficult because of the long-range nature of Coulombic forces.[35] In a slab geometry, the complexity increases further because of the reduced symmetry, which complicates the implementation of periodic boundary conditions using standard Ewald summation techniques. Different methods have been devised to overcome these difficulties.[36−41] Recently, we introduced a new method that allowed us to efficiently perform simulations of systems with an underlying slab geometry.[42] The method was developed specifically to study inhomogeneous Coulomb systems near charged surfaces, such as electrodes, membranes, or large colloidal particles. The idea of the new approach is to separate the electrostatic potential produced by the uniformly charged surface from the other electrostatic interactions, treating it as an external potential acting on ions and polyions. The difficulty, however, is that such a separation results in a non-neutral Coulomb system that, when treated using regular Ewald summation, leads to infinite electrostatic self-energy. Nevertheless, we were able to show that this infinite contribution can be renormalized away, resulting in a well-defined finite electrostatic energy that can be used within the Metropolis algorithm to very efficiently perform Monte Carlo (MC) simulations. A similar approach was also recently proposed in refs 43, 44 in which the regularization was done by introducing a uniform background. In the present article, we will show how to modify the energy expressions derived in ref 42 to study systems with dielectric discontinuities.[45]

A particularly interesting application of the new algorithm, presented in the present article, is to explore the adsorption of polyions onto a like-charged dielectric surface, which could

Received: June 14, 2016
Revised: September 6, 2016
Published: September 8, 2016

DOI: 10.1021/acs.jpcb.6b06002
J. Phys. Chem. B 2016, 120, 10387−10393

correspond to a phospholipid cell membrane, in an electrolyte solution containing multivalent and monovalent counterions. We will show how such systems can be efficiently simulated using the new algorithm based on the non-neutral three-dimensional (3D) Ewald summation method. In particular, we will explore the effects of dielectric surface polarization, multivalent counterions, and monovalent salts on the interaction between an anionic polyelectrolyte and a like-charged membrane. In the following sections, we will present the computational details, results, discussions, and conclusions of the present study. All technical details of the derivations will be provided in the Appendix.

COMPUTATIONAL DETAILS

Our system consists of a negatively charged surface with surface charge density σ, an anionic polyelectrolyte, and a dissolved salt. The simulation box has sides $L_x = 160.1$ Å, $L_y = L_x$, and $L_z = 4L_x$. The electrolyte is confined in $-L_x/2 < x < L_x/2$, $-L_y/2 < y < L_y/2$, and $0 < z < L$, where $L = 250$ Å, whereas empty space is maintained in the complementary region, $L < z < 4L_x$. The charged surface is located at $z = 0$. The primitive model is considered. The polyions are modeled as flexible linear chains of N_m spherical monomers of charge $-q$ adjacent to each other, where q is the proton charge. Besides ions from the α:1 salt at concentration ρ_S, where α is the cationic valence, additional monovalent counterions of charge q that neutralize the polyion and surface charge are also present. The effective diameter of all ions and monomers is set to 4 Å. Water is a continuum medium of dielectric constant $\varepsilon_w = 80\varepsilon_0$, where $\varepsilon_0 = 1$ is the dielectric constant of vacuum. The Bjerrum length, defined as $\lambda_B = q^2/\varepsilon_w k_B T$, is set to 7.2 Å, the value for water at room temperature. In the region of empty space, $z < 0$, we consider that the medium is a continuum with dielectric constant ε_m, modeling a cell membrane. The total energy of the system is given by

$$U = U_S + U_{self} + U_L + U_{cor} + U_P + U_{pol} \tag{1}$$

In the present method, the details of which are presented in the Appendix, the electrostatic interaction energy between an *infinite* charged dielectric surface and all of the charged particles is calculated explicitly and is given by

$$U_P = -\frac{2\pi}{\varepsilon_w}(1+\gamma)\sum_{i=1}^{N} q_i z_i \sigma \tag{2}$$

where $\gamma = (\varepsilon_w - \varepsilon_m)/(\varepsilon_w + \varepsilon_m)$. The rest of the polyelectrolyte−electrolyte system, which in the absence of the surface charge accounted for by eq 2 is no longer charge-neutral, is treated using our modified periodic 3D Ewald summation method. The Coulomb potential is split into short-range and long-range contributions. The short-range part can be studied using simple periodic boundary conditions, whereas the long-range contribution can be efficiently evaluated in the reciprocal Fourier space. The short-range electrostatic energy is

$$U_S = (1/2)\sum_{i=1}^{N} q_i \phi_i^S(\boldsymbol{r}_i) \tag{3}$$

where $\phi_i^S(\boldsymbol{r})$ is

$$\phi_i^S(\boldsymbol{r}) = \sum_{j=1}^{N}{}' q_j \frac{\mathrm{erfc}(\kappa_e|\boldsymbol{r}-\boldsymbol{r}_j|)}{\varepsilon_w|\boldsymbol{r}-\boldsymbol{r}_j|} + \sum_{j=1}^{N} \gamma q_j \frac{\mathrm{erfc}(\kappa_e|\boldsymbol{r}-\boldsymbol{r}_j'|)}{\varepsilon_w|\boldsymbol{r}-\boldsymbol{r}_j'|} \tag{4}$$

where N refers to all of the charges in the simulation box, except the wall charge; $\boldsymbol{r}_j$ is the position of charge q_j; and $\boldsymbol{r}_j' = \boldsymbol{r}_j - 2z_j\hat{\boldsymbol{z}}$ is the position of image charge γq_j. The prime on the summation means that $j \neq i$. The damping parameter is set to $\kappa_e = 4/L_x$. The self-energy contribution is

$$U_{self} = -(\kappa_e/\varepsilon_w\sqrt{\pi})\sum_{i=1}^{N} q_i^2 \tag{5}$$

The long-range electrostatic energy is

$$U_L = \sum_{\boldsymbol{k}\neq\boldsymbol{0}} \frac{2\pi}{\varepsilon_w V|\boldsymbol{k}|^2} \exp\left(-\frac{|\boldsymbol{k}|^2}{4\kappa_e^2}\right) \times [A(\boldsymbol{k})^2 + B(\boldsymbol{k})^2 + A(\boldsymbol{k})C(\boldsymbol{k}) + B(\boldsymbol{k})D(\boldsymbol{k})] \tag{6}$$

where

$$A(\boldsymbol{k}) = \sum_{i=1}^{N} q_i \cos(\boldsymbol{k}\cdot\boldsymbol{r}_i)$$

$$B(\boldsymbol{k}) = -\sum_{i=1}^{N} q_i \sin(\boldsymbol{k}\cdot\boldsymbol{r}_i)$$

$$C(\boldsymbol{k}) = \sum_{i=1}^{N} \gamma q_i \cos(\boldsymbol{k}\cdot\boldsymbol{r}_i')$$

$$D(\boldsymbol{k}) = -\sum_{i=1}^{N} \gamma q_i \sin(\boldsymbol{k}\cdot\boldsymbol{r}_i')$$

The number of vectors, $\boldsymbol{k}$, defined as $\boldsymbol{k} = (2\pi n_x/L_x, 2\pi n_y/L_y, 2\pi n_z/L_z)$, where n's are integers, is set to around 400 to achieve convergence.

The correction, which accounts for the conditional convergence of the Ewald summation appropriate for the slab geometry, is derived in the Appendix. It is given by

$$U_{cor} = \frac{2\pi}{\varepsilon_w V}[M_z^2(1-\gamma) - G_z Q_t(1+\gamma)] \tag{7}$$

where

$$M_z = \sum_{i=1}^{N} q_i z_i, \quad G_z = \sum_{i=1}^{N} q_i z_i^2, \quad \text{and } Q_t = \sum_{i=1}^{N} q_i \tag{8}$$

Note that this correction depends on the net charge, Q_t, present inside the simulation cell, without including the surface charge of the membrane, which has already been accounted for in U_P.

The monomers that compose a polyion interact via Coulomb potential and a simple parabolic potential[33,46,47] that models stretching of molecular bonds

$$U_{pol} = \sum_{\text{ad.mon.}} \frac{A}{2}(r - r_0)^2 \tag{9}$$

The sum is over the adjacent monomers, where r is the distance between the adjacent monomers, $A = 0.97 k_B T$, and $r_0 = 5$ Å.

The simulations are performed using the Metropolis algorithm, with 10^6 MC steps for equilibration. The profiles are calculated with 5×10^4 uncorrelated states, each obtained with 100 trial movements per particle. Polyions can perform rotations and reptation moves. In addition, polyion monomers can attempt short displacements, whereas ions can perform both short- and long-distance moves.

DOI: 10.1021/acs.jpcb.6b06002
J. Phys. Chem. B 2016, 120, 10387−10393

RESULTS AND DISCUSSION

First, we explore the effect of dielectric discontinuity on the interaction of a polyelectrolyte with a surface. We consider two cases: $\varepsilon_m = \varepsilon_w$ and $\varepsilon_m = \varepsilon_0$. The effect of surface polarization on the ionic double layer was extensively studied for different geometries.[48−57] In Figure 1, the polyion center of mass (PCM) distribution is shown as a function of the distance from the wall, for a system with $\alpha = 3$. We see that the effect of membrane polarization is surprisingly small. Although the multivalent counterions are strongly repelled from the surface (see Figure 2), the net effect on the polyion adsorption is minimal, with only a slight change in the equilibrium position of the PCM distribution. This small effect of the dielectric contrast is a consequence of the collapsed globular structure of the polyions, induced by the condensed multivalent counterions. This shape of the polyions results in the peak value of PCM being located at 12 Å (see Figure 1), which is quite far from the surface. Note that the density profile of trivalent ions for the same parameters peaks around 4 Å (see Figure 2). The large separation of the PCM of the condensed polyelectrolyte from the surface is responsible for the small effect that the dielectric contrast appears to have on the equilibrium position of the adsorbed polyions. In the following discussion, we will take into account the membrane polarization by setting $\varepsilon_m = \varepsilon_0$.

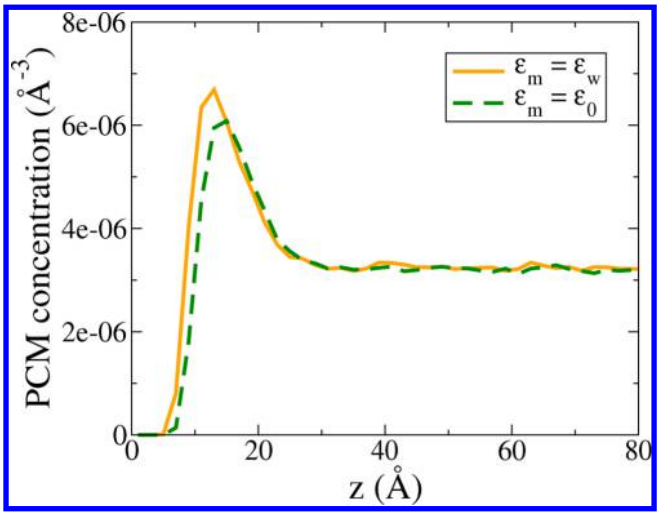

Figure 1. Comparison between the PCM concentration and the distance from the surface, obtained with $\varepsilon_m = \varepsilon_0$ and $\varepsilon_m = \varepsilon_w$, corresponding to the absence of polarization. Surface charge density $\sigma = -0.1$ C/m^2, the number of polyions in the simulation box is 20, $N_m = 18$, $\alpha = 3$, and the salt concentration is 60 mM.

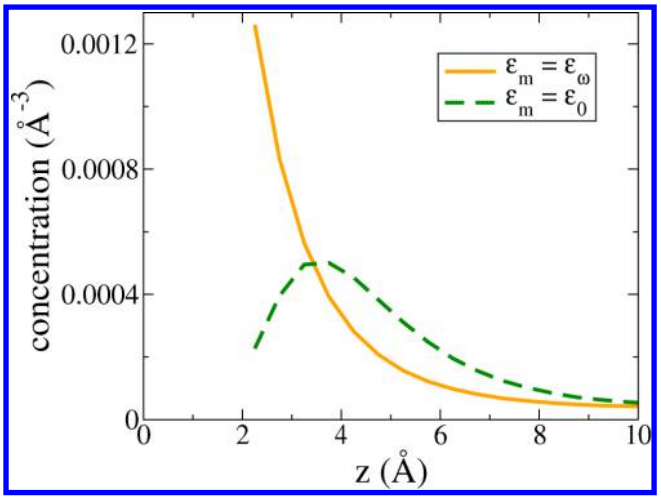

Figure 2. Trivalent cation concentration vs distance from the surface, obtained with and without surface polarization. The parameters are the same as those in Figure 1.

The effect of electrolyte concentration on adsorption is shown in Figure 3, in which the results are presented for $\alpha = 1$, 2, and 3. As can be seen, in the absence of electrolyte, the polyions do not adsorb onto a like-charged membrane. Increasing the concentration of the $\alpha = 1$ electrolyte enhances the electrostatic screening, decreasing the repulsion, leading to a small adsorption at a high salt concentration, in agreement with the recent experimental results.[34] The adsorption is a consequence of many body interactions between the surface-condensed counterions and the polyelectrolyte monomers. For the $\alpha = 2$ electrolyte, there is a significant adsorption of polyions onto a like-charged membrane, as was also observed in the experiments[34] and simulations.[32] Next, we consider the $\alpha = 3$ electrolyte. In this case, the adsorption of polyions is very strong, mediated by the positional correlations of the condensed multivalent counterions and the polyelectrolyte monomers, in agreement with the previous simulation results.[33] We also see that the adsorption decreases for sufficiently large concentrations of the $\alpha = 3$ electrolyte, which is again consistent with the experimental observations.[34] The non-monotonic decrease in adsorption is a consequence of the competitions between the nonlinear effects of counterion correlations and "linear" Debye screening, which decreases all electrostatic interactions. We expect the same behavior to occur for 2:1 electrolytes but at concentrations higher than the ones investigated in the present article. A similar effect has been found for colloidal systems, for which the effective colloidal charge was predicted to first decrease, and sometimes even become reversed, with increasing concentration of electrolyte, with the trend reversing at larger multivalent salt concentrations.[58] Finally, in Figure 4, we explore the effect of addition of a 1:1 electrolyte to a polyelectrolyte solution containing the $\alpha = 3$ electrolyte at 60 mM concentration. We see that the addition of the 1:1 electrolyte screens the electrostatic interactions, diminishing the adsorption of polyions onto a like-charged surface.[58]

The mechanism responsible for the attraction of the polyion to a like-charged membrane was partially attributed to hydrophobic interactions between the charged polymers and the surface, for moderate trivalent salt concentrations.[34] However, here, we see that purely electrostatic interactions, without any specific hydrophobic effects, already result in a like-charge attraction. It was also suggested[34] that the charge inversion of the polyion−cation complex is responsible for the polyion condensation onto a like-charged surface. However, our simulations show that, in general, this is not the case. In the presented model, the polyions are not sufficiently charged to result in a charge reversal of the polyion−cation complex. In simulations, we see that the attraction is a consequence of strong electrostatic correlations between the adsorbed multivalent ions[31,59,60] and the polyion monomers. Electrostatic correlations have been previously found to also be responsible for the reversal of electrophoretic mobility[61,62] and attraction between like-charged colloidal particles.[31,63]

DOI: 10.1021/acs.jpcb.6b06002
J. Phys. Chem. B 2016, 120, 10387−10393

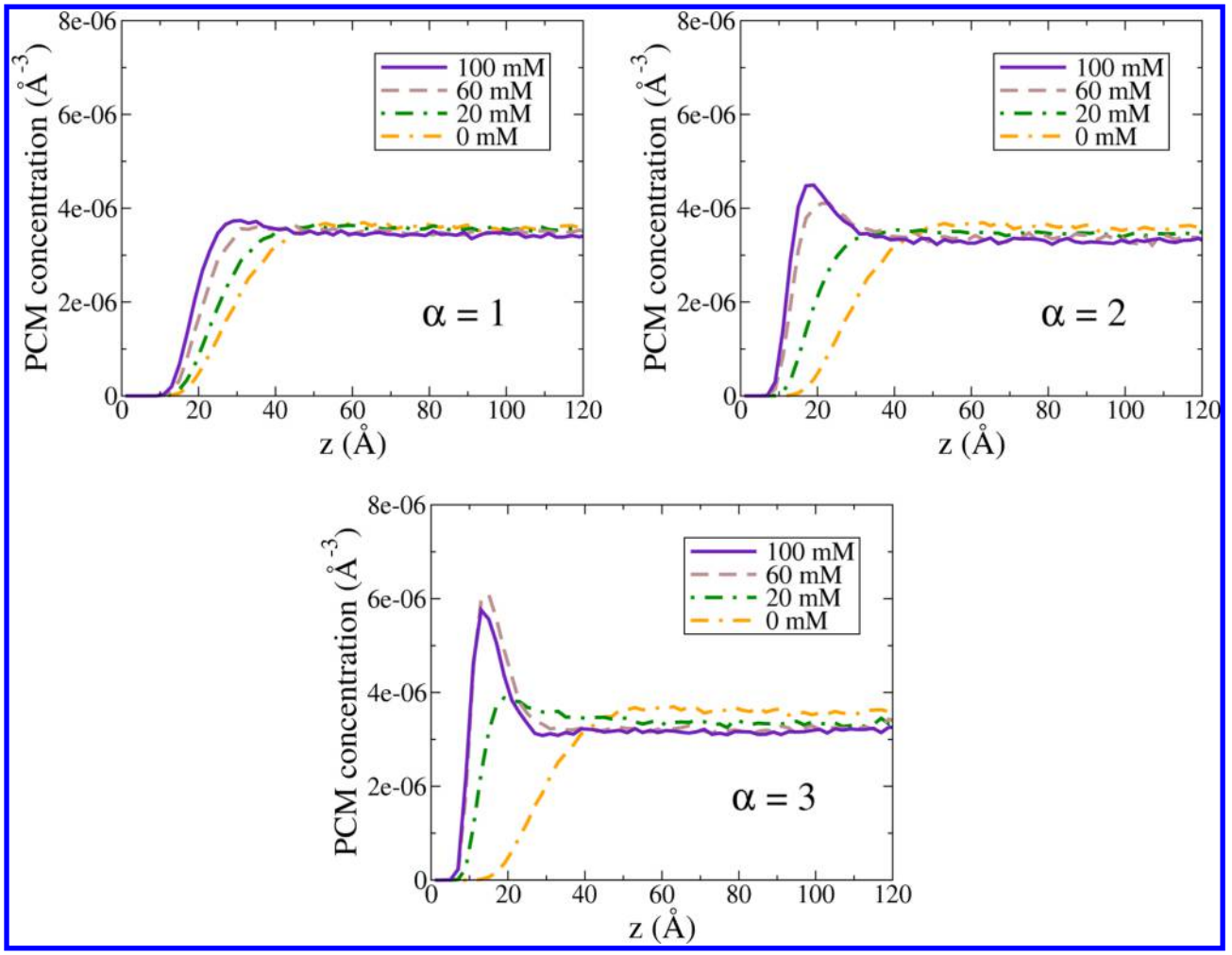

Figure 3. PCM concentration vs distance from the surface, obtained for different salt concentrations. The parameters are the same as those in Figure 1, except α and salt concentrations. The valence of the α:1 electrolyte is indicated in the panels.

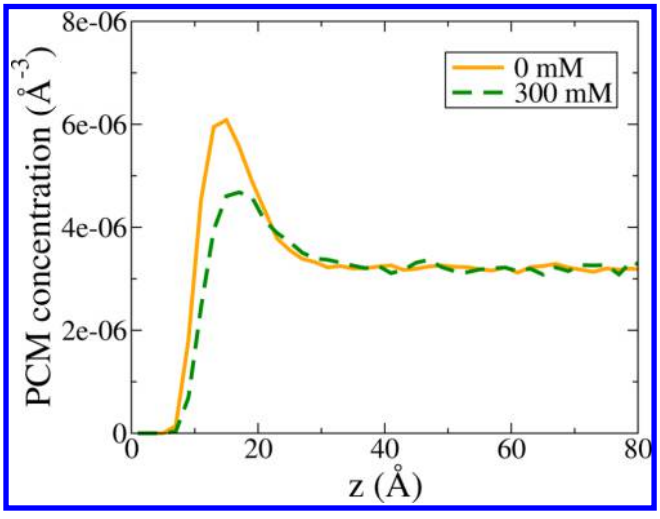

Figure 4. Comparison between the PCM density and distance from the surface, obtained with and without the addition of a 1:1 salt. The concentration of the 3:1 electrolyte is fixed at 60 mM. The parameters are the same as those in Figure 1.

CONCLUSIONS

We have presented MC simulations of polyelectrolyte solutions interacting with like-charged surfaces. The simulations were performed using a recently developed algorithm that allows us to efficiently study inhomogeneous Coulomb systems with a planar charged interface.[42] The effect of membrane polarization, which results in an induced surface charge, has been taken into account using image charges. The adsorption has been characterized by the PCM distribution. Surprisingly, we find a small adsorption of polyions onto a like-charged membrane even for the α = 1 electrolyte at a sufficiently high concentration. In this case, the electrostatic correlations do not play any significant role and the attraction is a consequence of steric and depletion interactions. For the α = 2 electrolyte, under all of the conditions studied in the article, adsorption increased with salt concentration; however, we expect this trend to reverse at concentrations higher than the ones explored in the present article, similar to that observed for trivalent counterions. For the α = 3 electrolyte, the polyion adsorption was found to first increase with the concentration of the multivalent salt and then decrease. Addition of a 1:1 electrolyte to a polyelectrolyte solution containing multivalent counterions decreased the polyion adsorption. All of the results are consistent with the recent experimental observations.

DOI: 10.1021/acs.jpcb.6b06002
J. Phys. Chem. B 2016, 120, 10387−10393

APPENDIX

Energy Calculations

We consider a system of N charged particles, with charges q_j located at $\boldsymbol{r}_j$, bounded by a dielectric wall at $z = 0$. The simulation box has sides L_x, L_y, and L_z and volume $V = L_xL_yL_z$. The electrolyte is confined in $-L_x/2 < x < L_x/2$, $-L_y/2 < y < L_y/2$, and $0 < z < L$. In general, the system is not charge-neutral. To take into account the long-range nature of Coulombic forces, we replicate the system periodically in all directions. The ions in the main simulation cell interact with all other ions in the cell and also with all periodic replicas. We define replication vector $\boldsymbol{r}_{rep}$ as (n_xL_x, n_yL_y, n_zL_z), where n's are integers. To correctly simulate the system, we have to consider the polarization of the dielectric wall, which can be done by introducing image charges. The potential due to the real and image charges at an arbitrary position, $\boldsymbol{r}$, inside the main simulation cell is

$$\phi_i(\boldsymbol{r}) = \sum_{\boldsymbol{n}}^{\infty}{}' \sum_{j=1}^{N} \int \frac{\rho_j(\boldsymbol{s})}{\varepsilon_w|\boldsymbol{r}-\boldsymbol{s}|}\,d^3\boldsymbol{s} + \sum_{\boldsymbol{n}}^{\infty} \sum_{j=1}^{N} \int \frac{\rho_j'(\boldsymbol{s})}{\varepsilon_w|\boldsymbol{r}-\boldsymbol{s}|}\,d^3\boldsymbol{s} \tag{10}$$

where $\rho_j(\boldsymbol{s}) = q_j\delta(\boldsymbol{s} - \boldsymbol{r}_j - \boldsymbol{r}_{rep})$ is the charge density of ion j and its infinite replicas and $\rho_j'(\boldsymbol{s}) = \gamma q_j\delta(\boldsymbol{s} - \boldsymbol{r}_j' - \boldsymbol{r}_{rep})$ is the image charge density of ion j and its infinite replicas. The prime over the summation means that $i \neq j$ for $\boldsymbol{n} = (0, 0, 0)$. Constant γ assumes the value $\gamma = (\varepsilon_w - \varepsilon_m)/(\varepsilon_w + \varepsilon_m)$, where ε_m is the dielectric constant of the surface medium and ε_w is the dielectric constant of the medium in which the real charges are. Vector $\boldsymbol{r}_j'$ is the position of the image charges defined as $\boldsymbol{r}_j' = \boldsymbol{r}_j - 2z_j\hat{\boldsymbol{z}}$. Vectors $\boldsymbol{n} = (n_x, n_y, n_z)$ represent the different replicas.

We use the 3D Ewald summation technique to efficiently sum over the replicas. The potential has the form

$$\begin{aligned}\phi_i(\boldsymbol{r}) = {} & \sum_{\boldsymbol{n}}^{\infty}{}' \sum_{j=1}^{N} \int \frac{\rho_j(\boldsymbol{s}) - \rho_j^{G}(\boldsymbol{s})}{\varepsilon_w|\boldsymbol{r}-\boldsymbol{s}|}\,d^3\boldsymbol{s} \\ & + \sum_{\boldsymbol{n}}^{\infty} \sum_{j=1}^{N} \int \frac{\rho_j'(\boldsymbol{s}) - \rho_j'^{G}(\boldsymbol{s})}{\varepsilon_w|\boldsymbol{r}-\boldsymbol{s}|}\,d^3\boldsymbol{s} \\ & + \sum_{\boldsymbol{n}}^{\infty} \sum_{j=1}^{N} \int \frac{\rho_j^{G}(\boldsymbol{s})}{\varepsilon_w|\boldsymbol{r}-\boldsymbol{s}|}\,d^3\boldsymbol{s} + \sum_{\boldsymbol{n}}^{\infty} \sum_{j=1}^{N} \int \frac{\rho_j'^{G}(\boldsymbol{s})}{\varepsilon_w|\boldsymbol{r}-\boldsymbol{s}|}\,d^3\boldsymbol{s} \\ & - \int \frac{\rho_i^{G}(\boldsymbol{s})}{\varepsilon_w|\boldsymbol{r}-\boldsymbol{s}|}\,d^3\boldsymbol{s}\end{aligned} \tag{11}$$

where

$$\begin{aligned}\rho_j^{G}(\boldsymbol{s}) &= q_j(\kappa_e^3/\sqrt{\pi^3})\exp(-\kappa_e^2|\boldsymbol{s} - \boldsymbol{r}_j - \boldsymbol{r}_{rep}|^2) \\ \rho_j'^{G}(\boldsymbol{s}) &= \gamma q_j(\kappa_e^3/\sqrt{\pi^3})\exp(-\kappa_e^2|\boldsymbol{s} - \boldsymbol{r}_j' - \boldsymbol{r}_{rep}|^2)\end{aligned} \tag{12}$$

and κ_e is a damping parameter. The first two terms of eq 11 define a short-range potential, $\phi_i^S(\boldsymbol{r})$

$$\phi_i^S(\boldsymbol{r}) = \sum_{j=1}^{N}{}' q_j \frac{\mathrm{erfc}(\kappa_e|\boldsymbol{r} - \boldsymbol{r}_j|)}{\varepsilon_w|\boldsymbol{r} - \boldsymbol{r}_j|} + \sum_{j=1}^{N} \gamma q_j \frac{\mathrm{erfc}(\kappa_e|\boldsymbol{r} - \boldsymbol{r}_j'|)}{\varepsilon_w|\boldsymbol{r} - \boldsymbol{r}_j'|} \tag{13}$$

Notice that we can exclude the summation over $\boldsymbol{n}$'s in the short-range potential, adopting the usual minimum image convention, $\boldsymbol{n} = (0, 0, 0)$. This is appropriate because of the exponentially fast decay of $\mathrm{erfc}(x)$ with increasing x. The total short-range interaction energy is then

$$U_S = (1/2)\sum_{i=1}^{N} q_i\phi_i^S(\boldsymbol{r}_i) \tag{14}$$

The last term of eq 11 is added to remove the prime over the summation in the third term of eq 11 and corresponds to the potential produced by the ith Gaussian charge

$$\phi_i^{self}(\boldsymbol{r}) = q_i \frac{\mathrm{erf}(\kappa_e|\boldsymbol{r} - \boldsymbol{r}_i|)}{\varepsilon_w|\boldsymbol{r} - \boldsymbol{r}_i|} \tag{15}$$

The total self-energy is

$$U_{self} = -\frac{1}{2}\sum_{i=1}^{N} q_i\phi_i^{self}(\boldsymbol{r}_i) = -\frac{\kappa_e}{\varepsilon_w\sqrt{\pi}}\sum_{i=1}^{N} q_i^2 \tag{16}$$

The third and fourth terms of eq 11 define the long-range potential, $\phi_i^L(\boldsymbol{r})$

$$\begin{aligned}\phi^L(\boldsymbol{r}) = {} & \sum_{\boldsymbol{n}}^{\infty} \sum_{j=1}^{N} q_j \frac{\mathrm{erf}(\kappa_e|\boldsymbol{r} - \boldsymbol{r}_j - \boldsymbol{r}_{rep}|)}{\varepsilon_w|\boldsymbol{r} - \boldsymbol{r}_j - \boldsymbol{r}_{rep}|} \\ & + \sum_{\boldsymbol{n}}^{\infty} \sum_{j=1}^{N} \gamma q_j \frac{\mathrm{erf}(\kappa_e|\boldsymbol{r} - \boldsymbol{r}_j' - \boldsymbol{r}_{rep}|)}{\varepsilon_w|\boldsymbol{r} - \boldsymbol{r}_j' - \boldsymbol{r}_{rep}|}\end{aligned} \tag{17}$$

We can Fourier-transform eq 17, resulting in

$$\begin{aligned}\phi^L(\boldsymbol{r}) = {} & \sum_{\boldsymbol{k}=\boldsymbol{0}}^{\infty} \sum_{j=1}^{N} \frac{4\pi q_j}{\varepsilon_w V|\boldsymbol{k}|^2} \exp\left[-\frac{|\boldsymbol{k}|^2}{4\kappa_e^2}\right][\exp[i\boldsymbol{k}\cdot(\boldsymbol{r} - \boldsymbol{r}_j)] \\ & + \gamma \exp[i\boldsymbol{k}\cdot(\boldsymbol{r} - \boldsymbol{r}_j')]]\end{aligned} \tag{18}$$

with $\boldsymbol{k} = \left(\frac{2\pi}{L_x}n_x, \frac{2\pi}{L_y}n_y, \frac{2\pi}{L_z}n_z\right)$. We note that the term corresponding to $\boldsymbol{k} = (0, 0, 0)$ is divergent. However, the divergence can be renormalized away by changing the zero point of the potential, as discussed in ref 42. We expand the singular term around $\boldsymbol{k} = (0, 0, 0)$ and keep the nonvanishing factors

$$\begin{aligned}\lim_{\boldsymbol{k}\to 0} \sum_{j=1}^{N} \frac{4\pi q_j}{\varepsilon_w V}\Bigg[& \frac{1}{|\boldsymbol{k}|^2} - \frac{1}{4\kappa_e^2} + \frac{i\boldsymbol{k}\cdot(\boldsymbol{r} - \boldsymbol{r}_j)}{|\boldsymbol{k}|^2} + \gamma\frac{i\boldsymbol{k}\cdot(\boldsymbol{r} - \boldsymbol{r}_j')}{|\boldsymbol{k}|^2} \\ & - \frac{[\boldsymbol{k}\cdot(\boldsymbol{r} - \boldsymbol{r}_j)]^2}{2|\boldsymbol{k}|^2} - \gamma\frac{[\boldsymbol{k}\cdot(\boldsymbol{r} - \boldsymbol{r}_j')]^2}{2|\boldsymbol{k}|^2}\Bigg]\end{aligned} \tag{19}$$

The first two terms are zero for neutral systems, $\sum_{j=1}^{N} q_j = 0$, but diverge for systems with a net charge. However, they are independent of position and can be renormalized away by simply redefining the zero of the potential.[42] The second and third terms are zero, as shown in ref 42. The remaining terms can be calculated taking into account the aspect ratio of the infinite system. For details of the calculations, see ref 42. For a slab geometry, the directions $\hat{\boldsymbol{x}}$ and $\hat{\boldsymbol{y}}$ tend to infinity much faster than $\hat{\boldsymbol{z}}$, resulting in a finite correction potential

$$\phi_i^{cor}(\boldsymbol{r}) = -\sum_{j=1}^{N} \frac{2\pi q_j}{\varepsilon_w V}[(z - z_j)^2 + \gamma(z - z_j')^2] \tag{20}$$

The correction energy is $U_{cor} = (1/2)\sum_{i=1}^{N} q_i\phi_i^{cor}(\boldsymbol{r}_i)$, which after a short calculation reduces to

DOI: 10.1021/acs.jpcb.6b06002
J. Phys. Chem. B 2016, 120, 10387−10393

$$U_{cor} = \frac{2\pi}{\varepsilon_w V}[M_z^2(1-\gamma) - G_z Q_t(1+\gamma)] \tag{21}$$

where

$$M_z = \sum_{i=1}^{N} q_i z_i, \quad G_z = \sum_{i=1}^{N} q_i z_i^2, \quad \text{and } Q_t = \sum_{i=1}^{N} q_i \tag{22}$$

We can now exclude $\boldsymbol{k} = \mathbf{0}$ in the long-range potential (eq 18), as it is now accounted for by the correction potential. The long-range energy is given by $U_L = (1/2)\sum_{i=1}^{N} q_i \phi_i^L(\boldsymbol{r}_i)$, which can be written as

$$U_L = \sum_{\boldsymbol{k}\neq\mathbf{0}} \frac{2\pi}{\varepsilon_w V|\boldsymbol{k}|^2} \exp\left(-\frac{|\boldsymbol{k}|^2}{4\kappa_e^2}\right) \times [A(\boldsymbol{k})^2 + B(\boldsymbol{k})^2 + A(\boldsymbol{k})C(\boldsymbol{k}) + B(\boldsymbol{k})D(\boldsymbol{k})] \tag{23}$$

where

$$A(\boldsymbol{k}) = \sum_{i=1}^{N} q_i \cos(\boldsymbol{k}\cdot\boldsymbol{r}_i)$$

$$B(\boldsymbol{k}) = -\sum_{i=1}^{N} q_i \sin(\boldsymbol{k}\cdot\boldsymbol{r}_i)$$

$$C(\boldsymbol{k}) = \sum_{i=1}^{N} \gamma q_i \cos(\boldsymbol{k}\cdot\boldsymbol{r}_i')$$

$$D(\boldsymbol{k}) = -\sum_{i=1}^{N} \gamma q_i \sin(\boldsymbol{k}\cdot\boldsymbol{r}_i')$$

In general, charged surfaces also contribute with counterions, which must be included in the main simulation cell. The electrostatic potential produced by the surface acts on all of the charged particles inside the simulation cell and can be added as an external field

$$\phi_p(\boldsymbol{r}) = -\frac{2\pi}{\varepsilon_w}(1+\gamma)\sigma z \tag{24}$$

where σ is the surface charge density. The total plate ions' interaction energy is $U_P = \sum_{i=1}^{N} q_i \phi_P(\boldsymbol{r}_i)$.

The total electrostatic energy is given by a sum of all contributions

$$U = U_S + U_{self} + U_{cor} + U_L + U_P \tag{25}$$

AUTHOR INFORMATION

Corresponding Authors

*E-mail: alexandre.pereira@ufrgs.br. Tel: 55 51 33086517 (A.P.d.S.).
*E-mail: matheus.girotto@ufrgs.br (M.G.).
*E-mail: levin@if.ufrgs.br (Y.L.).

Notes

The authors declare no competing financial interest.

ACKNOWLEDGMENTS

This work was partially supported by the CNPq, INCT-FCx, and the US-AFOSR under grant FA9550-16-1-0280.

REFERENCES

(1) Bajdur, W.; Pajaczkowska, J.; Makarucha, B.; Sulkowska, A.; Sulkowski, W. W. Effective Polyelectrolytes Synthesised from Expanded Polystyrene Wastes. *Eur. Polym. J.* **2002**, *38*, 299−304.
(2) Wang, M. H.; Janout, V.; Regen, S. L. Gas Transport across Hyperthin Membranes. *Acc. Chem. Res.* **2013**, *46*, 2743−2754.
(3) Cakmak, I.; Ulukanli, Z.; Tuzcu, M.; Karabuga, S.; Genctav, K. Synthesis and Characterization of Novel Antimicrobial Cationic Polyelectrolytes. *Eur. Polym. J.* **2004**, *40*, 2373−2379.
(4) Lu, L. D.; Rininsland, F. H.; Wittenburg, S. K.; Achyuthan, K. E.; McBranch, D. W.; Whitten, D. G. Biocidal Activity of a Light-Absorbing Fluorescent Conjugated Polyelectrolyte. *Langmuir* **2005**, *21*, 10154−10159.
(5) Kiss, É.; Heine, E. T.; Hill, K.; He, Y. C.; Keusgen, N.; Pénzes, C. B.; Schnöller, D.; Gyulai, G.; Mendrek, A.; Keul, H.; et al. Membrane Affinity and Antibacterial Properties of Cationic Polyelectrolytes with Different Hydrophobicity. *Macromol. Biosci.* **2012**, *12*, 1181−1189.
(6) Hoque, J.; Akkapeddi, P.; Yarlagadda, V.; Uppu, D. S. S. M.; Kumar, P.; Haldar, J. Cleavable Cationic Antibacterial Amphiphiles: Synthesis, Mechanism of Action, and Cytotoxicities. *Langmuir* **2012**, *28*, 12225−12234.
(7) Falentin-Daudré, C.; Faure, E.; Svaldo-Lanero, T.; Farina, F.; Jérôme, C.; Van De Weerdt, C.; Martial, J.; Duwez, A. S.; Detrembleur, C. Antibacterial Polyelectrolyte Micelles for Coating Stainless Steel. *Langmuir* **2012**, *28*, 7233−7241.
(8) Feng, X. L.; Liu, L. B.; Wang, S.; Zhu, D. B. Water-Soluble Fluorescent Conjugated Polymers and their Interactions with Biomacromolecules for Sensitive Sensors. *Chem. Soc. Rev.* **2010**, *39*, 2411−2419.
(9) Kim, H. N.; Guo, Z. Q.; Zhu, W. H.; Yoon, J.; Tian, H. Recent Progress on Polymer-Based Fluorescent and Colorimetric Chemosensors. *Chem. Soc. Rev.* **2011**, *40*, 79−93.
(10) Kong, C. Y.; Muthukumar, M. Monte Carlo Study of a Polyelectrolyte onto Charged Surfaces. *J. Chem. Phys.* **1998**, *109*, 1522−1557.
(11) Chodanowski, P.; Stoll, S. Polyelectrolyte Adsorption on Charged Particles: Ionic Concentration and Particle Size Effects−A Monte Carlo Approach. *J. Chem. Phys.* **2001**, *115*, 4951−4960.
(12) Dobrynin, A. V.; Deshkovski, A.; Rubinstein, M. Adsorption of Polyelectrolytes at an Oppositely Charged Surface. *Phys. Rev. Lett.* **2000**, *84*, 3101−3104.
(13) Dobrynin, A. V.; Deshkovski, A.; Rubinstein, M. Adsorption of Polyelectrolytes at Oppositely Charged Surfaces. *Macromolecules* **2001**, *34*, 3421−3436.
(14) Dobrynin, A. V.; Rubinstein, M. Adsorption of Hydrophobic Polyelectrolytes at Oppositely Charged Surfaces. *Macromolecules* **2002**, *35*, 2754−2768.
(15) McNamara, J.; Kong, C. Y.; Muthukumar, M. Monte Carlo Studies of Adsorption of a Sequenced Polyelectrolyte to Patterned Surfaces. *J. Chem. Phys.* **2002**, *117*, 5354−5360.
(16) Reddy, G.; Yethiraj, A. Solvent Effects in Polyelectrolyte Adsorption: Computer Simulations with Explicit and Implicit Solvent. *J. Chem. Phys.* **2010**, *132*, No. 074903.
(17) Qiao, B.; Cerdà, J. J.; Holm, C. Atomistic Study of Surface Effects on Polyelectrolyte Adsorption: Case Study of a Poly(styrenesulfonate) Monolayer. *Macromolecules* **2011**, *44*, 1707−1718.
(18) Faraudo, J.; Martin-Molina, A. Competing Forces in the Interaction of Polyelectrolytes with Charged Surfaces. *Curr. Opin. Colloid Interface Sci.* **2013**, *18*, 517−523.
(19) Stoll, S.; Chodanowski, P. Polyelectrolyte Adsorption on an Oppositely Charged Spherical Particle. Chain Rigidity Effects. *Macromolecules* **2002**, *35*, 9556−9562.
(20) Messina, R.; Holm, C.; Kremer, K. Polyelectrolyte Adsorption and Multilayering on Charged Colloidal Particles. *J. Polym. Sci., Part B: Polym. Phys.* **2004**, *42*, 3557−3570.
(21) Salomaki, M.; Kankare, J. Specific Anion Effect in Swelling of Polyelectrolyte Multilayers. *Macromolecules* **2008**, *41*, 4423−4428.

DOI: 10.1021/acs.jpcb.6b06002
J. Phys. Chem. B 2016, 120, 10387−10393

(22) dos Santos, A. P.; Levin, Y. Adsorption of Cationic Polyions onto a Hydrophobic Surface in the Presence of Hofmeister Salts. *Soft Matter* **2013**, *9*, 10545−10549.
(23) Kou, R.; Zhang, J.; Wang, T.; Liu, G. Interactions between Polyelectrolyte Brushes and Hofmeister Ions: Chaotropes versus Kosmotropes. *Langmuir* **2015**, *31*, 10461−10468.
(24) Ha, B. Y.; Liu, A. J. Counterion-Mediated, Non-Pairwise-Additive Attractions in Bundles of Like-Charged Rods. *Phys. Rev. E* **1999**, *60*, 803−813.
(25) Arenzon, J. J.; Stilck, J. F.; Levin, Y. Simple Model for Attraction between Like-Charged Polyions. *Eur. Phys. J. B* **1999**, *12*, 79−82.
(26) Deserno, M.; Jiménez-Ángeles, F.; Holm, C.; Lozada-Cassou, M. Overcharging of DNA in the Presence of Salt: Theory and Simulation. *J. Phys. Chem. B* **2001**, *105*, 10983−10991.
(27) Butler, J. C.; Angelini, T.; Tang, J. X.; Wong, G. C. L. Ion Multivalence and Like-Charged Polyelectrolyte Attraction. *Phys. Rev. Lett.* **2003**, *91*, No. 028301.
(28) Deserno, M.; Arnold, A.; Holm, C. Attraction and Ionic Correlations between Charged Stiff Polyelectrolytes. *Macromolecules* **2003**, *36*, 249−259.
(29) Angelini, T. E.; Liang, H.; Wriggers, W.; Wong, G. C. L. Like-Charge Attraction between Polyelectrolytes Induced by Counterion Charge Density Waves. *Proc. Natl. Acad. Sci. U.S.A.* **2003**, *100*, 8634−8637.
(30) Molnar, F.; Rieger, J. "Like-Charge Attraction" between Anionic Polyelectrolytes: Molecular Dynamics Simulations. *Langmuir* **2005**, *21*, 786−789.
(31) Levin, Y. Electrostatic Correlations: from Plasma to Biology. *Rep. Prog. Phys.* **2002**, *65*, 1577−1632.
(32) Turesson, M.; Labbez, C.; Nonat, A. Calcium Mediated Polyelectrolyte Adsorption on Like-Charged Surfaces. *Langmuir* **2011**, *27*, 13572−13581.
(33) Luque-Caballero, G.; Martín-Molina, A.; Quesada-Pérez, M. Polyelectrolyte Adsorption onto Like-Charged Surfaces Mediated by Trivalent Counterions: A Monte Carlo Simulation Study. *J. Chem. Phys.* **2014**, *140*, No. 174701.
(34) Tiraferri, A.; Maroni, P.; Borkovec, M. Adsorption of Polyelectrolyte to Like-Charged Substrates Induced by Multivalent Counterions as Exemplified by Poly(styrene sulfonate) and Silica. *Phys. Chem. Chem. Phys.* **2015**, *17*, 10348−10352.
(35) Allen, M. P.; Tildesley, D. J. *Computer Simulations of Liquid*; Oxford: Oxford University Press: New York, 1987.
(36) Torrie, G. M.; Valleau, J. P. Electrical Double Layers. I. Monte Carlo Study of a Uniformly Charged Surface. *J. Chem. Phys.* **1980**, *73*, 5807−5816.
(37) Torrie, G. M.; Valleau, J. P.; Outhwaite, C. W. Electrical Double Layers. VI. Image effects for Divalent Ions. *J. Chem. Phys.* **1984**, *81*, 6296−6300.
(38) Lekner, J. Summation of Coulomb Fields in Computer-Simulated Disordered Systems. *Physica A* **1991**, *176*, 485−498.
(39) Widmann, A. H.; Adolf, D. B. A Comparison of Ewald Summation Techniques for Planar Surfaces. *Comput. Phys. Commun.* **1997**, *107*, 167−186.
(40) Yeh, I.; Berkowitz, M. L. Ewald Summation for Systems with Slab Geometry. *J. Chem. Phys.* **1999**, *111*, 3155−3162.
(41) Arnold, A.; Holm, C. A Novel Method for Calculating Electrostatic Interaction in 2D Periodic Slab Geometry. *Chem. Phys. Lett.* **2002**, *354*, 324−330.
(42) dos Santos, A. P.; Girotto, M.; Levin, Y. Simulations of Coulomb Systems with Slab Geometry Using an Efficient 3D Ewald Summation Method. *J. Chem. Phys.* **2016**, *144*, No. 144103.
(43) Ballenegger, V.; Arnold, A.; Cerdà, J. J. Simulation of Non-Neutral Slab Systems with Long-Range Electrostatic Interactions in Two-Dimensional Periodic Boundary Conditions. *J. Chem. Phys.* **2009**, *131*, No. 094107.
(44) Ballenegger, V. Communication: On the Origin of the Surface Term in the Ewald Formula. *J. Chem. Phys.* **2014**, *140*, No. 161102.
(45) dos Santos, A. P.; Levin, Y. *Electrostatics of Soft and Disordered Matter*; CRC Press: Boca Raton, FL, 2014; Chapter 14.
(46) Dias, R. S.; Pais, A. A. C. C.; Linse, P.; Miguel, M. G.; Lindman, B. Polyion Adsorption onto Catanionic Surfaces. A Monte Carlo Study. *J. Phys. Chem. B* **2005**, *109*, 11781−11788.
(47) Quesada-Pérez, M.; Martín-Molina, A. Monte Carlo Simulation of Thermo-Responsive Charged Nanogels in Salt-Free Solutions. *Soft Matter* **2013**, *9*, 7086−7094.
(48) Kanduc, M.; Naji, A.; Podgornik, R. Counterion-Mediated Weak and Strong Coupling Electrostatic Interaction between Like-Charged Cylindrical Dielectrics. *J. Chem. Phys.* **2010**, *132*, No. 224703.
(49) Nagy, T.; Henderson, D.; Boda, D. Simulation of an Electrical Double Layer Model with a Low Dielectric Layer between the Electrode and the Electrolyte. *J. Phys. Chem. B* **2011**, *115*, 11409−11419.
(50) Šamaj, L.; Trizac, E. Counterions at Highly Charged Interfaces: From One Plate to Like-Charge Attraction. *Phys. Rev. Lett.* **2011**, *106*, No. 078301.
(51) Bakhshandeh, A.; dos Santos, A. P.; Levin, Y. Weak and Strong Coupling Theories for Polarizable Colloids and Nanoparticles. *Phys. Rev. Lett.* **2011**, *107*, No. 107801.
(52) dos Santos, A. P.; Bakhshandeh, A.; Levin, Y. Effects of the Dielectric Discontinuity on the Counterion Distribution in a Colloidal Suspension. *J. Chem. Phys.* **2011**, *135*, No. 044124.
(53) Diehl, A.; dos Santos, A. P.; Levin, Y. Surface Tension of an Electrolyte-Air Interface: a Monte Carlo Study. *J. Phys.: Condens. Matter* **2012**, *24*, No. 284115.
(54) Lue, L.; Linse, P. Macroion Solutions in the Cell Model Studied by Field Theory and Monte Carlo Simulations. *J. Chem. Phys.* **2011**, *135*, No. 224508.
(55) Wang, R.; Wang, Z. G. Effects of Image Charges on Double Layer Structure and Forces. *J. Chem. Phys.* **2013**, *139*, No. 124702.
(56) Jing, Y. F.; Jadhao, V.; Zwanikken, J. W.; de la Cruz, M. O. Ionic Structure in Liquids Confined by Dielectric Interfaces. *J. Chem. Phys.* **2015**, *143*, No. 194508.
(57) dos Santos, A. P.; Levin, Y. Electrolytes between Dielectric Charged Surfaces: Simulations and Theory. *J. Chem. Phys.* **2015**, *142*, No. 194104.
(58) Pianegonda, S.; Barbosa, M. C.; Levin, Y. Charge Reversal of Colloidal Particles. *Europhys. Lett.* **2005**, *71*, 831−837.
(59) Shklovskii, B. I. Screening of a Macroion by Multivalent Ions: Correlation-Induced Inversion of Charge. *Phys. Rev. E* **1999**, *60*, 5802−5811.
(60) dos Santos, A. P.; Diehl, A.; Levin, Y. Electrostatic Correlations in Colloidal Suspensions: Density Profiles and Effective Charges beyond the Poisson-Boltzmann Theory. *J. Chem. Phys.* **2009**, *130*, No. 124110.
(61) Quesada-Pérez, M.; Callejas-Fernández, J.; Hidalgo-Álvarez, R. Interaction Potentials, Structural Ordering and Effective Charges in Dispersions of Charged Colloidal Particles. *Adv. Colloid Interface Sci.* **2002**, *95*, 295−315.
(62) Fernández-Nieves, A.; Fernández-Barbero, A.; de las Nieves, F. J.; Vincent, B. Ionic Correlations in Highly Charge-Asymmetric Colloidal Liquids. *J. Chem. Phys.* **2005**, *123*, No. 054905.
(63) Solis, F. J.; de la Cruz, M. O. Flexible Polymers Also Counterattract. *Phys. Today* **2001**, *54*, 71−72.

DOI: 10.1021/acs.jpcb.6b06002
J. Phys. Chem. B 2016, 120, 10387−10393